

UC Berkeley

UC Berkeley Previously Published Works

Title

Non-invasive imaging of cellulose microfibril orientation within plant cell walls by polarized Raman microspectroscopy

Permalink

<https://escholarship.org/uc/item/8cb725c6>

Journal

Biotechnology and Bioengineering, 113(1)

ISSN

0006-3592

Authors

Sun, Lan

Singh, Seema

Joo, Michael

et al.

Publication Date

2016

DOI

10.1002/bit.25690

Peer reviewed

1Non-Invasive Imaging of Cellulose Microfibril 2Orientation within Plant Cell Walls by Polarized 3Raman Microspectroscopy

4Lan Sun^{1ab,2}, Seema Singh^{1b,2}, Michael Joo^{3b}, Miguel Vega-Sanchez^{1c,3a,#}, Pamela Ronald^{1c,4}, Blake
5A. Simmons^{1b,2}, Paul Adams^{1a,3a,5}, Manfred Auer^{1a,3b*}

6^{1a}Technology Division, ^{1b}Deconstruction Division, ^{1c}Feedstocks Division, Joint BioEnergy

7Institute, Lawrence Berkeley Laboratory, 5885 Hollis Street, Emeryville, CA94608

8²Biological and Engineering Sciences Center, Sandia National laboratories, P.O. Box 969,

9Livermore, CA 94551

10^{3a}Physical Biosciences Division, ^{3b}Life Sciences Division, Lawrence Berkeley Laboratory, One

11Cyclotron Road, Berkeley, CA 94720

12⁴Department of Plant Pathology and the Genome Center, University of California, Davis, One

13Shields Ave., Davis, CA 95616

14⁵Department of Bioengineering, University of California, Berkeley, 306 Stanley Hall, Berkeley,

15CA 94720

16*Corresponding Author: Manfred Auer

17Address: Life Sciences Division, Lawrence Berkeley Laboratory, One Cyclotron Road,
18Berkeley, CA 94720; Phone: 510-486-7702; Fax: 510-486-6488; Email: mauer@lbl.gov

19#Current affiliation: Monsanto Company, Chesterfield Village, Chesterfield, MO 63017

20Running Title: Raman imaging of Cellulose Microfibril Orientation

21ABSTRACT

22Cellulose microfibrils represent the major scaffold of plant cell walls. Different packing and
23orientation of the microfibrils at the microscopic scale determines the macroscopic properties of
24cell walls and thus affect their functions with a profound effect on plant survival. We developed
25a polarized Raman microspectroscopic method to determine cellulose microfibril orientation
26within rice plant cell walls. Employing an array of point measurements as well as area imaging
27and subsequent Matlab-assisted data processing, we were able to characterize the distribution of
28cellulose microfibril orientation in terms of director angle and anisotropy magnitude. Using this
29approach we detected differences between wild type rice plants and the rice *brittle culm* mutant,
30which shows a more disordered cellulose microfibril arrangement, and differences between
31different tissues of a wild type rice plant. This novel non-invasive Raman imaging approach
32allows for quantitative assessment of cellulose fiber orientation in cell walls of herbaceous
33plants, an important advancement in cell wall characterization.

34KEYWORDS: Cellulose microfibril orientation, polarized Raman microspectroscopy, plant cell
35wall, *brittle culm* mutant, director angle, anisotropy magnitude

36

37

38

39

40

41INTRODUCTION

42Cellulose microfibrils represent the major scaffold of plant cell walls. Multiple strands of
43repeating β -1-4 linking cellobiose units are closely arranged into a filamentous structure, also
44known as cellulose microfibrils. Their packing into ordered arrays and supramolecular
45organization at the microscopic scale determines the macroscopic mechanical properties of cell
46walls and thus affects their functions with a profound effect on plant survival (Booker and Sell
471998), and with high significance for many industrial applications (Goswami et al. 1996;
48Madakadze et al. 1999; Varanasi et al. 2012). Due to this importance of cellulose microfibril
49orientation for cell wall properties, non-invasive measurement techniques that allow
50determination of microfibril organization are highly desirable by plant biologists and industrial
51users of plant materials in order to better understand and control the physical properties of these
52materials.

53 Cellulose microfibril orientation is often described by the term microfibril angle (MFA)
54in wood science, referring to the angle between the direction of the helical windings of cellulose
55microfibrils in the secondary cell wall of fibers and tracheids and the long axis of the cell. A
56review article by [Donaldson \(2008\)](#) presents a comprehensive summary of techniques to measure
57MFA and divides them into two categories, either measurement of individual tracheids or fibers
58using microscopy or measurement of bulk wood samples using X-ray diffraction or near infrared
59(NIR) spectroscopy. Polarization microscopy (Palviainen et al. 2004; Ye 2006), differential
60interference contrast (DIC) microscopy (Peter et al. 2003), scanning electron microscopy (Abe et
61al. 1991), and transmission electron microscopy (Donaldson and Xu 2005) are some
62representative microscopic techniques for MFA measurement. Furthermore biological, chemical

63or physical treatments of wood samples have been adopted by some researchers to help visualize
64the orientation of the microfibrils, such as iodine staining (Donaldson and Frankland 2005) and
65ultrasonic treatment (Huang 1995). X-ray diffraction is currently perhaps the most popular
66method for measuring MFA, and given its simplicity can be applied to a single wall or to strips
67of wood several millimeters in thickness, and thus is very convenient for determining average
68MFA (Barnett and Bonham 2004; Cave 1997). NIR spectroscopy can be used to estimate MFA
69among a range of other wood properties for a large number of wood samples based on
70calibrations established by the measured physical properties (Schimleck et al. 2001a; Schimleck
71et al. 2001b). MFA predicted by NIR was found to be in excellent agreement with MFA
72determined by X-ray diffractometry (Schimleck and Evans 2002).

73 Although these measurement techniques have been used to measure MFA of individual
74fibers or bulk wood samples, limited work has been done to investigate the distribution of
75cellulose microfibril orientation within cell walls. Position-resolved property determination is
76important for a variety of applications, as the distribution of MFA within different layers of cell
77walls, cell walls of different tissues, and cell walls from different parts of a plant may vary
78significantly, resulting in differences in overall wood properties (Barnett and Bonham 2004). For
79example, for biofuel production, researchers are engineering lignocellulosic feedstocks for easier
80deconstruction. However, the effect on mechanical **strength** of the plant cannot be easily
81predicted. Therefore, the distribution of MFA within cell walls and across different cell types can
82be used to evaluate and predict mechanical **strength** of these mutant plants, which will ultimately
83allow researchers to make predictions for their survival in the wild/field. However, in order to
84acquire this position-resolved information, microscopic imaging with sufficient spatial resolution

85is required. Attempts have been made to study the helical arrangement of cellulose fibrils in the
86S2 layer of adjacent wood cells using synchrotron X-ray imaging (Lichtenegger et al. 1999).
87However, this tool is often not easily accessible due to the limited number of facilities that have a
88synchrotron light source. In addition, the X-ray beam size of 2 μm is not small enough to provide
89high-resolution imaging within individual cell walls. Infrared imaging, another promising
90approach for studying cell wall organization, can be used to acquire position-resolved chemical
91compositions of plant cell walls (Dokken et al. 2005). However, due to the low sensitivity caused
92by non-background-free detection, the low spatial resolution associated with the long infrared
93wavelengths, and water absorption of the infrared light, this technique is somewhat limited
94(Evans and Xie 2008).

95 In contrast to the limitations posed by these approaches, Raman microspectroscopy offers
96several attractive advantages. First, nondestructive measurements with strong chemical
97selectivity and specificity **towards major cell wall components** can be performed with minimum
98sample preparation and without any interference from water. Second, submicron spatial
99resolutions can be achieved to provide tissue and cell type specific compositional information
100about cell walls (Agarwal 2006; Gierlinger and Schwanninger 2006; Sun et al. 2013; Sun et al.
1012011). Third, by controlling the polarization direction of the incoming excitation laser,
102orientation information about the cell wall components can be acquired. Therefore, due to the
103chemical selectivity and specificity of this technique, this approach has the potential to monitor
104both the structural and chemical changes of the cell walls, including plant biomass that was
105chemically or genetically modified. In addition, unlike the limited access to a synchrotron light

106source, commercial and home built Raman microspectroscopy instruments are available to a
107broad scientific community.

108 Point measurement of macromolecular orientation in fibers and plant cell walls by
109polarized Raman spectroscopy was demonstrated in earlier studies (Agarwal and Atalla 1986;
110Atalla and Agarwal 1985; Atalla et al. 1980; Cao et al. 2006; Kovur et al. 2008). In a more recent
111study, Gierlinger et al. (2010) established a partial least square (PLS) regression model between
112the spectral intensity ratio and the angle of laser polarization for black spruce to predict MFA
113distribution based on spectra extracted from Raman images of black spruce cell walls. However,
114this approach relied on a PLS model that was developed based on a single fiber, and the Raman
115images were only collected with two incident laser polarization directions perpendicular to each
116other. To obtain accurate prediction of the MFA distribution in cell walls, a perfect perpendicular
117alignment between the fiber axis and the cross-sectional area for the model fiber and a perfect
118parallel alignment between the radial or tangential cell walls with the laser polarization direction
119were required, which was difficult to accomplish in that study. Also, the differences between the
120model fiber and the cell wall specimen may cause inaccurate prediction of MFA in the cell wall,
121since the polarization-angle-dependent Raman profile can vary from pixel to pixel.

122 In this work, we performed polarized Raman microspectroscopy to study the spatial
123distribution of cellulose microfibril orientation in rice cell walls. Instead of using just two laser
124polarization directions, we performed a complete polarization-resolved procedure by collecting
12536 Raman images at 10° intervals around the excitation polarization direction. This approach is
126not impacted by heterogeneity of the angle-resolved Raman profile from pixel to pixel caused by
127heterogeneity of cell wall compositions at different positions, since the angle-resolved Raman

128profile is generated at every pixel independently and calculation is not relying on calibration
129models obtained using calibration samples different from the specimen of interest. Thus, this
130approach can be used to determine cellulose microfibril orientation at different positions in cell
131walls more accurately. In addition, we overcame the significant challenge of data processing for
132complete polarization-resolved Raman imaging by developing Matlab codes to process a large
133number of data sets simultaneously (Matlab code is available upon request). Through this
134technique, we observed clear differences in cellulose microfibril orientation between different
135tissues of the wild type rice plant as well as between the wild type and the *brittle culm* mutant, a
136mutant compromised in secondary cell wall deposition.

137MATERIALS AND METHODS

138Materials and Sample Preparation

139Wild type rice and *brittle culm* (*bc*) rice mutant were used for this study. The mutant (RGT3584-
140bc) and wild type control (a segregant line not containing the transposon insertion: RGT3584-
141WT) are in the cultivar Nipponbare background and were obtained from the Rice Insertional
142Mutation Database, Sundaresan Lab at UC Davis. The RGT3584-bc mutant contains an Ac/Ds
143transposon insertion in the locus of the rice *OsCesA7* gene, which encodes for a subunit of the
144Cellulose Synthase (CESA) complex involved in the biosynthesis of cellulose in secondary cell
145walls of rice (Tanaka et al. 2003). We have previously shown that this mutant contains both
146reduced cellulose content (Smith-Moritz et al. 2011) and severely compromised mechanical
147strength (Varanasi et al. 2012). Plants were grown in growth chambers as described in Vega-
148Sanchez et al. (2012), and samples were collected at the full senescence stage.

149 The senesced, dry leaf sheath sections were hand cut into small pieces and directly used
150 for point measurement. For Raman imaging, dry plant samples were embedded in LR white resin
151 using a protocol similar to transmission electron microscopy, except that samples did not
152 undergo any fixation or heavy metal staining. Samples were dehydrated at room temperature in a
153 graded aqueous ethanol series (25%, 50%, 75%, v/v, 3 min for each step) followed by three
154 incubations (5 min each) in 100% ethanol. Samples were infiltrated with LR White resin in a
155 graded LR White/ethanol series (25%, 50%, 75% v/v, 3 min for each step) followed by three
156 incubations (5 min each) in 100 % resin. After polymerization at 65°C for 2 days, a LR White
157 embedded sample was first cut in half longitudinally so that the closed, hollow cylindrical shape
158 became an open U-shaped structure, which was then sectioned longitudinally with an
159 ultramicrotome (Leica, Buffalo Grove, IL). The sections from the ultramicrotome were thin
160 rectangles at a nominal thickness of 500 nm or 1 μm . These sections were transferred to glass
161 slides for Raman imaging.

162 Polarized Raman Microspectroscopy

163 All the measurements were performed using a LabRam HR 800 confocal Raman system
164 equipped with a 785 nm laser (Horiba Jobin Yvon, Edison, NJ). A high numerical aperture 100 \times
165 (oil NA 1.40) objective was used to acquire all the spectra. For point measurement of the leaf
166 sheath sections, integration time was 20 s for the wild type plant and 80 s for the *brittle culm*
167 mutant, respectively. For imaging, a marked area of 2.5 μm by 3.0 μm was scanned at a mapping
168 step of 0.5 μm with an integration time of 3 s for the leaf sheath section. A marked area of 1.0
169 μm by 3.0 μm was scanned at a mapping step of 0.5 μm with an integration time of 5 s for the
170 stem and leaf sections. The estimated laser spot size was $\sim 0.7 \mu\text{m}$. The laser penetration depth

171 was very sample dependent and the maximum penetration would probably be about 5 to 10 μm .
172 The raster mapping technique was utilized in SWIFT mode (the stage triggers the detector at
173 specific positions and acquisition is done “on the fly”) to significantly increase mapping speed.
174 The grating was 300 g/mm and the spectral resolution was $\sim 11 \text{ cm}^{-1}$. The polarization direction
175 of the excitation laser was changed in increments of 10° by rotating the half-wave plate
176 manually. Both point measurements and Raman imaging were performed at every polarization
177 direction ranging from 0° to 360° at an interval of 10° .

178

179 Data Processing

180 The raw Raman spectra in the range of interest were pre-processed using the LabSpec5 software
181 (Horiba Jobin Yvon, Edison, NJ), which sequentially removes spikes, corrects baselines,
182 smoothes the spectra by the Savitsky-Golay algorithm at a moderate level, and then further
183 smoothes the data by Fourier transformation coupled with cosine apodization function. A
184 Matlab code (the code is available upon request) was developed to determine intensity at the
185 characteristic peak of interest and perform ellipse fitting to determine the two parameters that
186 define the fiber orientation, director angle and anisotropy magnitude, for all measurement
187 positions. Here, for each position (x, y) in the plant section for measurement, the maximum
188 intensity as a function of excitation polarization is denoted by $I_{\text{max}}(x, y)$, and the orientation of the
189 excitation polarization associated with this intensity is indicated by $\phi_{\text{max}}(x, y)$, the director angle.
190 The minimum intensity as a function of excitation polarization is denoted by $I_{\text{min}}(x, y)$. $I_{\text{max}}(x, y)$
191 and $I_{\text{min}}(x, y)$ can be determined by ellipse fitting of the intensity data as a function of excitation

192polarization. Thus, the anisotropy magnitude, $\rho(x, y)$, can be calculated by Equation 1
193(Zimmerley et al. 2010)

$$194 \quad \rho(x, y) = \frac{I_{\max|x,y|} - I_{\min|x,y|}}{I_{\max|x,y|} + I_{\min|x,y|}} \quad (1)$$

195RESULTS AND DISCUSSION

196We utilized the orientation dependency of the characteristic Raman peak of cellulose in order to
197determine the cellulose microfibril orientation. The experimental set-up is shown in Figure 1.
198The polarization direction of the excitation laser was controlled by a half-wave plate. When the
199half-wave plate is rotated 1 θ degree, polarization of the incident laser is rotated 2 θ degree. In
200this study, the rotation step (θ) was 5 degrees and data was therefore collected every 10 degrees.
201In principle, when the cellulose microfibril orientation is parallel to the polarization direction of
202the excitation laser, the maximum Raman intensity of the characteristic cellulose peak will be
203obtained. When the cellulose microfibril orientation is perpendicular to the polarization direction
204of the excitation laser, the minimum Raman intensity of the same peak will be obtained. Thus, by
205ellipse fitting of the intensity data as a function of excitation polarization, we determined the
206maximum and minimum Raman intensity of the characteristic cellulose peak and hence the
207cellulose microfibril orientation.

208 To demonstrate the concept of detection, we used a longitudinal leaf sheath section of
209wild type (RGT3584-WT, cv. Nipponbare) rice as a model system. Raman spectra in the range of
210200-1700 cm^{-1} as a function of polarization direction of the excitation laser are shown in Figure
2112a. It can be clearly seen in the zoomed-in spectral range of 1017-1218 cm^{-1} (see Figure 2b) that
212the intensity of the two major cellulose peaks, 1095 cm^{-1} and 1122 cm^{-1} , assigned to backbone

213stretching (Wiley and Atalla 1987), was changing with the change of polarization direction of the
214excitation laser. We observed a more significant change at 1095 cm^{-1} , as confirmed by ellipse
215fitting of the peak intensity as a function of the polarization direction of the excitation laser for
216both cellulose peaks (see Figure 2c, d). $I_{\max}(x, y)$ and $I_{\min}(x, y)$ are the long and short axes of the
217fitted ellipses, respectively, and the anisotropy magnitudes can then be calculated accordingly as
218the ratio of the differences between $I_{\max}(x, y)$ and $I_{\min}(x, y)$ over the sum of $I_{\max}(x, y)$ and $I_{\min}(x,$
219y). The anisotropy magnitude of the peak at 1095 cm^{-1} ($\rho = 0.21$) is significantly higher than that
220of the peak at 1122 cm^{-1} ($\rho = 0.09$), indicating that the peak at 1095 cm^{-1} has a stronger
221dependence on excitation polarization. Thus, this peak was used in this study to determine
222cellulose microfibril orientation, and for this particular cell wall position, the director angle in
223wild type was found to be 30° (see Figure 2c). In addition to the cellulose peak, we also tested
224the dependence on excitation polarization of the lignin peak at 1600 cm^{-1} , assigned to symmetric
225stretching of the aromatic ring (Atalla and Agarwal 1985; Atalla and Agarwal 1986). As shown
226in Figure 2e, we did not observe a significant dependence of Raman intensity at 1600 cm^{-1} as a
227function of changes in the direction of excitation polarization, indicating that there is no
228preferred orientation of aromatic rings of lignin in the longitudinal plane of the leaf sheath
229section of the wild type rice plant. Our result for lignin is similar to previous observations in the
230latewood fiber of spruce (*Picea abies*) (Gierlinger et al. 2010), but is different from previous
231results obtained from the secondary wall in early wood tissue of black spruce (*Picea mariana*)
232(Atalla and Agarwal 1985). It should be noted that there was negligible contribution of signal
233from LR white for the spectral ranges of interest in this work. Since we were using low grating

234(300 g/mm) in this work, the differences in grating's reflectivity at different polarization
235direction were negligible.

236 Using the method described above, we conducted the first study, to our knowledge, that
237uses polarized Raman microspectroscopy to detect differences of cellulose microfibril orientation
238in cell walls between wild type and mutant herbaceous plants. We focused on leaf sheath
239sections of wild type and *brittle culm* rice plants as our model samples. Grass *brittle culm*
240mutants display compromised mechanical strength properties in diverse plant tissues and are
241associated with defects in cellulose biosynthesis and/or deposition in the plant cell wall (Zhang
242and Zhou 2011). Field emission scanning electron microscopy had previously been used to
243examine the innermost secondary walls of wild type and *brittle culm 12 (bc12)* rice plants and
244showed that wild-type fibers were packed in a parallel pattern, whereas those of the mutant
245plants were arranged in a random manner. Combined with additional compositional analysis of
246cell walls, the study concluded that the inferior mechanical strength of *bc12* is probably caused
247by the altered wall composition and aberrantly deposited cellulose microfibrils in the secondary
248walls (Zhang et al. 2010). However, previous work characterizing herbaceous plant mutants had
249to measure composition and packing pattern of the cellulose microfibrils separately and hence
250was not able to obtain these two pieces of information from the same section of a sample. Also,
251previous work was not able to provide quantitative information about cellulose microfibril
252orientation. Our proposed method, on the other hand, can directly and quantitatively reveal the
253differences between wild type and mutant plants in both compositional information and
254microfibril orientation at the specified location within the plant cell walls.

255 As shown in Figure 3, we observed differences in microfibril orientation when comparing
256 leaf sheath samples between wild type and *bc* rice plants using point measurements. We marked
257 six points in a single cell wall of the wild type and mutant samples in the bright field images (see
258 Figure 3a, c) for polarized Raman measurements (see Figure 3b, d). By plotting the Raman
259 intensity at 1095 cm⁻¹ as a function of polarization direction of the excitation laser and ellipse
260 fitting, we determined the director angle and thus the cellulose microfibril orientation at specific
261 positions within the cell wall (see Figure 3b, d). For the wild type sample, we determined the
262 director angle as 20° between the cellulose microfibrils and the longitudinal axis of the cell wall.
263 The director angle was relatively constant for each of the measured points in the cell wall,
264 indicating an ordered overall arrangement of the cellulose microfibrils. In contrast, we did not
265 observe any constant director angle for the positions within the cell wall of the *brittle culm*
266 mutant sample, indicating a more random arrangement of the cellulose microfibrils. The distinct
267 differences in the cellulose microfibril orientation between the wild type and mutant plants were
268 also evident from significant difference in the anisotropy magnitude (see Figure 3b, d). **The**
269 ***brittle culm* mutant was determined previously to have compromised mechanical strength**
270 **(Varanasi et al. 2012), indicating that cellulose microfibril orientation in cell walls might be**
271 **related with mechanical strength of plants.** It should be noted that while an integration time of 20
272 s was used for the wild type plant, due to low cellulose signal we used a significantly longer
273 integration time (80 s) for the mutant plant. This indicates that cellulose content was significantly
274 reduced in the mutant, which is consistent with previous observation (Smith-Moritz et al. 2011;
275 Tanaka et al. 2003).

276 Using a similar concept as demonstrated above, we were able to reveal the spatial
277 distribution of cellulose microfibril orientation within plant cell walls in terms of director angle,
278 $\phi_{\max}(x, y)$, as well as anisotropy magnitude, $\rho(x, y)$, by Raman microspectroscopy or Raman
279 imaging that has the advantages of high spatial resolution and chemical specificity. Essentially,
280 we first chose the area of interest within the cell wall and generated grids for imaging. Then we
281 scanned the marked area by collecting Raman spectra from each position on the mapping grids.
282 We repeated the same procedure at every polarization direction of the excitation laser and thus
283 generated 36 Raman maps. It took less than 2 h to collect all of these 36 maps with our setting.
284 We didn't observe much drift ($< 0.5 \mu\text{m}$, the mapping step) over time for the thin and flat section
285 for imaging, and thus our data acquisition/processing method does not account for drift. This
286 polarization-resolved imaging approach is not limited by heterogeneity of the polarization profile
287 from pixel to pixel and can determine cellulose microfibril orientation more accurately.
288 However, this approach posed a big challenge for data processing, since we had to obtain the
289 Raman intensity of the cellulose peak at every polarization direction from each mapping
290 position, perform ellipse fitting at all of the positions, and generate the corresponding graphs. It
291 is not realistic to perform this procedure manually and the commercial Raman imaging software
292 does not provide the functionality to do this analysis. To meet this challenge, we developed our
293 own Matlab codes to realize automatic data processing.

294 In order to map out microfibril orientation at high spatial resolution, we made
295 measurements at 42 positions at an interval of $0.5 \mu\text{m}$ in a leaf sheath section of the wild type
296 rice plant (see Figure 4 a, b). Each of the polar plots in Figure 4c corresponds to a specific
297 position marked in the bright field image. The director angle between cellulose microfibrils and

298the longitudinal axis of the plant section at this position was determined by ellipse fitting (red
299line) of the measured data (blue circles). For the same positions, a quiver plot can be obtained as
300shown in Figure 4d where the arrow orientation indicates the director angle and the length of the
301arrow indicates the corresponding anisotropy magnitude. We found the director angle to be **either**
302**20° or 30°** for the 42 positions measured. The anisotropy magnitude is quite uniformly
303distributed with an average of 0.24 and a standard deviation of 0.02. These results suggest that
304cellulose microfibrils are organized with a high degree of order within the leaf sheath cell walls.

305 We further utilized polarized Raman imaging in order to compare different tissues of the
306wild type rice plant. As illustrated in Figure 5, we measured the Raman signal for cellulose and
307lignin at 21 positions at an interval of 0.5 μm in a stem section and a leaf section of the wild type
308rice plant, respectively. Director angle and anisotropy magnitude of the stem and leaf sections
309are shown in the quiver plots in Figure 5. The detailed data for cellulose microfibril orientation
310are summarized in Table 1. The director angle was **either 20° or 30°** for the 21 positions
311measured in the stem section, while it was **either 10° or 20°** for the 21 positions measured in the
312leaf section with an exception (30°) at one position, which is slightly narrower than the stem
313section. We observed a higher value for the anisotropy magnitude in stem section (average =
3140.22, standard deviation = 0.02) compared to the leaf section (average = 0.14, standard deviation
315= 0.02), indicating a higher degree of order of the cellulose microfibrils in the stem section, with
316a cellulose microfibril orientation being very close to the value we obtained in the leaf sheath
317section. In addition to cellulose orientation, we also examined lignin orientation, and found that
318there was no preferred orientation of aromatic rings of lignin in the longitudinal plane of either

319the stem section or the leaf section of the wild type rice plant, consistent with our previous
320observation in the wild type leaf sheath section (see Figure 2e).

321 The current work is a proof-of-concept study. The proposed approach can be applied to
322different plant species, different tissue and cell types. Also, changes of fiber orientation caused
323by different physical, chemical and biochemical treatments can be monitored for different
324industrial applications. To increase the speed of data acquisition, measurement could be
325performed at polarization direction from 0° to 90° instead of 0° to 360° given the data quality
326presented in this study.

327

328CONCLUSIONS

329In this study, we have demonstrated the use of polarized Raman microspectroscopy to measure
330the spatial distribution of cellulose microfibril orientation within cell walls of rice, which is a
331fundamental property determining mechanical strength of cell walls and was insufficiently
332studied in the past due to limitation of measurement techniques. We determined both the director
333angle - the angle between the cellulose microfibrils and the longitudinal axis of the cell wall, as
334well as the anisotropy magnitude - the degree of fiber organization. Utilizing this method, we
335were able to determine differences in cellulose microfibril orientation between wild type and
336mutant rice plants and between different tissues of a wild type rice plant. To the best of our
337knowledge, this is the first time that polarized Raman microspectroscopy or Raman imaging was
338used to determine the spatial distribution of cellulose microfibril orientation within cell walls of
339herbaceous plants and to compare cellulose microfibril orientation in cell walls between wild

340type and mutant plants. This method can be readily extended to other plant species for both
341fundamental studies and applied (e.g. biofuel) applications.

342ACKNOWLEDGMENT

343This work conducted by the Joint BioEnergy Institute was supported by the Office of Science,
344Office of Biological and Environmental Research of the U.S. Department of Energy under
345contract no. DE-AC02-05CH11231. There are no potential sources of conflict of interest.

346

347REFERENCES

348Abe H, Ohtani J, Fukazawa K. 1991. FE-SEM observations on the microfibrillar orientation in
349 the secondary wall of tracheids. IAWA Bulletin n.s. 12(4):431-438.

350Agarwal U. 2006. Raman imaging to investigate ultrastructure and composition of plant cell
351 walls: distribution of lignin and cellulose in black spruce wood (*Picea mariana*). *Planta*
352 224(5):1141-1153.

353Agarwal UP, Atalla RH. 1986. In-situ Raman microprobe studies of plant cell walls:
354 Macromolecular organization and compositional variability in the secondary wall of
355 *Picea mariana* (Mill.) B.S.P. *Planta* 169(3):325-332.

356Atalla RH, Agarwal UP. 1985. Raman Microprobe Evidence for Lignin Orientation in the Cell
357 Walls of Native Woody Tissue. *Science* 227(4687):636-638.

358Atalla RH, Agarwal UP. 1986. Recording Raman spectra from plant cell walls. *Journal of Raman*
359 Spectroscopy 17(2):229-231.

- 360Atalla RH, Whitmore RE, Heimbach CJ. 1980. Raman Spectral Evidence for Molecular
361 Orientation in Native Cellulosic Fibers. *Macromolecules* 13(6):1717-1719.
- 362Barnett JR, Bonham VA. 2004. Cellulose microfibril angle in the cell wall of wood fibres.
363 *Biological Reviews* 79(2):461-472.
- 364Booker RE, Sell J. 1998. The nanostructure of the cell wall of softwoods and its functions in a
365 living tree. *Holz als Roh- und Werkstoff* 56(1):1-8.
- 366Cao Y, Shen D, Lu Y, Huang Y. 2006. A Raman-scattering Study on the Net Orientation of
367 Biomacromolecules in the Outer Epidermal Walls of Mature Wheat Stems (*Triticum*
368 *aestivum*). *Ann. Bot.* 97(6):1091-1094.
- 369Cave ID. 1997. Theory of X-ray measurement of microfibril angle in wood. *Wood Science and*
370 *Technology* 31(3):143-152.
- 371Dokken KM, Davis LC, Marinkovic NS. 2005. Use of Infrared Microspectroscopy in Plant
372 Growth and Development. *Appl. Spectrosc. Rev.* 40(4):301 - 326.
- 373Donaldson L. 2008. Microfibril angle: measurement, variation and relationships - a review.
374 *IAWA Journal* 29(4):345-386.
- 375Donaldson L, Frankland A. 2005. Ultrastructure of iodine treated wood. *Holzforschung*
376 58(3):219-225.
- 377Donaldson L, Xu P. 2005. Microfibril orientation across the secondary cell wall of Radiata pine
378 tracheids. *Trees: Structure and Function* 19(6):644-653.
- 379Evans CL, Xie XS. 2008. Coherent Anti-Stokes Raman Scattering Microscopy: Chemical
380 Imaging for Biology and Medicine. *Annual Review of Analytical Chemistry* 1(1):883-
381 909.

382Gierlinger N, Luss S, König C, Konnerth J, Eder M, Fratzl P. 2010. Cellulose microfibril
383 orientation of *Picea abies* and its variability at the micron-level determined by Raman
384 imaging. *J. Exp. Bot.* 61(2):587-595.

385Gierlinger N, Schwanninger M. 2006. Chemical Imaging of Poplar Wood Cell Walls by
386 Confocal Raman Microscopy. *Plant Physiol.* 140(4):1246-1254.

387Goswami T, Saikia CN, Baruah RK, Sarma CM. 1996. Characterization of pulp obtained from
388 *Populus deltoides* plants of different ages using IR, XRD and SEM. *Bioresour. Technol.*
389 57(2):209-214.

390Huang C-L. 1995. Revealing Fibril Angle in Wood Sections By Ultrasonic Treatment. *Wood and*
391 *Fiber Science* 27(1):49-54.

392Kovur SK, Schenzel K, Diepenbrock W. 2008. Orientation Dependent FT Raman
393 Microspectroscopy on Hemp Fibers. *Macromolecular Symposia* 265(1):205-210.

394Lichtenegger H, Müller M, Paris O, Riekkel C, Fratzl P. 1999. Imaging of the helical arrangement
395 of cellulose fibrils in wood by synchrotron X-ray microdiffraction. *Journal of Applied*
396 *Crystallography* 32(6):1127-1133.

397Madakadze IC, Radiotis T, Li J, Goel K, Smith DL. 1999. Kraft pulping characteristics and pulp
398 properties of warm season grasses. *Bioresour. Technol.* 69(1):75-85.

399Palviainen J, Silvennoinen R, Rouvinen J. 2004. Analysis of microfibril angle of wood fibers
400 using laser microscope polarimetry. *Optical Engineering* 43(1):186-191.

401Peter GF, Benton DM, Bennett K. 2003. A simple, direct method for measurement of microfibril
402 angle in single fibres using differential interference contrast microscopy. *Journal of Pulp*
403 *and Paper Science* 29(8):274-280.

404Schimleck L, Evans R, Ilic J. 2001a. Application of near infrared spectroscopy to a diverse range
405 of species demonstrating wide density and stiffness variation. *IAWA Journal* 22(4):415-
406 429.

407Schimleck LR, Evans R. 2002. Estimation of microfibril angle of increment cores by near
408 infrared spectroscopy. *IAWA Journal* 23(3):225-234.

409Schimleck LR, Evans R, Ilic J. 2001b. Estimation of *Eucalyptus delegatensis* wood properties by
410 near infrared spectroscopy. *Canadian Journal of Forest Research* 31(10):1671-1675.

411Smith-Moritz AM, Chern M, Lao J, Sze-To WH, Heazlewood JL, Ronald PC, Vega-Sánchez
412 ME. 2011. Combining multivariate analysis and monosaccharide composition modeling
413 to identify plant cell wall variations by Fourier Transform Near Infrared spectroscopy.
414 *Plant Methods* C7 - 26 7(1):1-13.

415Sun L, Li C, Xue Z, Simmons BA, Singh S. 2013. Unveiling high-resolution, tissue specific
416 dynamic changes in corn stover during ionic liquid pretreatment. *RSC Advances*
417 3(6):2017-2027.

418Sun L, Simmons BA, Singh S. 2011. Understanding tissue specific compositions of bioenergy
419 feedstocks through hyperspectral Raman imaging. *Biotechnol. Bioeng.* 108(2):286-295.

420Tanaka K, Murata K, Yamazaki M, Onosato K, Miyao A, Hirochika H. 2003. Three Distinct
421 Rice Cellulose Synthase Catalytic Subunit Genes Required for Cellulose Synthesis in the
422 Secondary Wall. *Plant Physiol.* 133(1):73-83.

423Varanasi P, Katsnelson J, Larson DM, Sharma R, Sharma MK, Vega-Sánchez ME, Zemla M,
424 Loque D, Ronald PC, Simmons BA and others. 2012. Mechanical stress analysis as a

425 method to understand the impact of genetically engineered rice and arabidopsis plants.
426 *Industrial Biotechnology* 8(4):238-244.

427 Vega-Sanchez ME, Verhertbruggen Y, Christensen U, Chen X, Sharma V, Varanasi P, Jobling
428 SA, Talbot M, White RG, Joo M and others. 2012. Loss of Cellulose Synthase-Like F6
429 function affects mixed-linkage glucan deposition, cell wall mechanical properties and
430 defense responses in vegetative tissues of rice. *Plant Physiol.*

431 Wiley JH, Atalla RH. 1987. Band assignments in the raman spectra of celluloses. *Carbohydrate*
432 *Research* 160:113-129.

433 Ye C. 2006. Spectroscopic imaging ellipsometry: real-time measurement of single, intact wood
434 pulp fibers. *Appl. Opt.* 45(36):9092-9104.

435 Zhang B, Zhou Y. 2011. Rice Brittleness Mutants: A Way to Open the ‘Black Box’ of Monocot
436 Cell Wall Biosynthesis Free Access. *Journal of Integrative Plant Biology* 53(2):136-142.

437 Zhang M, Zhang B, Qian Q, Yu Y, Li R, Zhang J, Liu X, Zeng D, Li J, Zhou Y. 2010.
438 Brittle Culm 12, a dual-targeting kinesin-4 protein, controls cell-cycle progression and
439 wall properties in rice. *The Plant Journal* 63(2):312-328.

440 Zimmerley M, Younger R, Valenton T, Oertel DC, Ward JL, Potma EO. 2010. Molecular
441 Orientation in Dry and Hydrated Cellulose Fibers: A Coherent Anti-Stokes Raman
442 Scattering Microscopy Study. *The Journal of Physical Chemistry B* 114(31):10200-
443 10208.

444
445
446

447**Table 1.** Summary of director angle and anisotropy magnitude of the stem and leaf sections of
 448the wild type rice plant.

Positions	Wild Type Rice Stem						Wild Type Rice Leaf					
	Director Angle*			Anisotropy Magnitude			Director Angle			Anisotropy Magnitude		
	1	2	3	1	2	3	1	2	3	1	2	3
1	30	30	20	0.21	0.21	0.24	20	10	20	0.13	0.14	0.11
2	20	30	20	0.22	0.19	0.24	20	20	20	0.14	0.14	0.12
3	30	20	20	0.15	0.23	0.22	20	20	20	0.18	0.12	0.16
4	20	20	20	0.22	0.24	0.22	20	20	20	0.17	0.13	0.14
5	20	20	30	0.22	0.21	0.24	20	20	30	0.09	0.17	0.11
6	30	20	20	0.23	0.18	0.24	20	10	20	0.13	0.13	0.13
7	20	20	20	0.23	0.23	0.20	20	20	20	0.14	0.13	0.14
Average	20			0.22			20			0.14		
SD [#]	0			0.02			0			0.02		

449* The resolution of director angle measurement was 10° in this work.

450[#] SD means standard deviation.

451

452

453

454

455

456

458LIST OF FIGURES

459**Figure 1.** Schematic of the experimental set-up. (a) Polarization direction of the incident laser is
460rotated 2θ when the half-wave plate is rotated θ . The step of θ is 5 degrees. The red arrow
461indicates the polarization direction of the laser beam. (b) The longitudinal section of the plant
462material is mounted on the stage of an inversed microscope. The red arrow indicates the
463polarization direction of the excitation laser.

464**Figure 2.** Determination of **cellulose and lignin** orientation at a single position in a leaf sheath
465sample of wild type (RGT3584-WT) rice. (a) Raman spectra in the spectral range of 200-1700
466 cm^{-1} ; (b) Raman spectra in the zoomed-in spectral range of 1017-1218 cm^{-1} after baseline
467correction in this range, where peaks at 1095 cm^{-1} and 1122 cm^{-1} are major cellulose peaks. (c)
468Determination of cellulose microfibril orientation using polar plot drawn from intensity data at
4691095 cm^{-1} ; (d) Determination of cellulose microfibril orientation using polar plot drawn from
470intensity data at 1122 cm^{-1} ; (e) Determination of lignin orientation using polar plot drawn from
471intensity data at 1600 cm^{-1} . In the polar plots, the blue circles denote the measured data, the red
472lines are the results of ellipse fitting, and ρ is the anisotropy magnitudes determined by the
473lengths of the long and short axes of the fitted ellipses in (c)-(e).

474**Figure 3.** Point measurements of leaf sheath samples of wild type (RGT3584-WT) and *brittle*
475*culm* (RGT3584-bc) mutant rice plants. (a) Bright field images of the wild type sample with six
476different positions marked for measurement; (b) Polar plots of Raman signals at 1095 cm^{-1}
477collected from these six different positions in the wild type sample, where ρ indicates the

478 corresponding anisotropy magnitude at these positions; (c) Bright field images of the *brittle culm*
479 sample with six different positions marked for measurements; (d) Polar plots of Raman signals at
480 1095 cm^{-1} collected from these six different positions in the *brittle culm* sample, where ρ
481 indicates the corresponding anisotropy magnitude at these positions.

482 **Figure 4.** Determination of cellulose microfibril orientation within leaf sheath section of wild
483 type (RGT3584-WT) rice sample by Raman microspectroscopy. (a) Bright field image of the leaf
484 sheath section with the marked area for measurement. (b) Blow-up image of the marked area. (c)
485 Polar plots of Raman intensity at 1095 cm^{-1} obtained from individual positions of the leaf sheath
486 section. (d) Quiver plot of distribution of cellulose microfibril orientation within the measured
487 area. In the polar plots, the blue circles denote the measured data and the red lines are the results
488 of ellipse fitting. In the quiver plot, the arrow direction indicates the director angle at the
489 specific position in the image and the length of the arrow indicates the corresponding anisotropy
490 magnitude.

491 **Figure 5.** Distribution of biopolymer orientation within the cell walls of (a) wild type
492 (RGT3584-WT) rice stem and (b) rice leaf. Top: bright images of selected areas for imaging;
493 Bottom left: Quiver plots of cellulose orientation; Bottom right: Quiver plots of lignin
494 orientation. In the quiver plots, the arrow direction indicates the director angle at the specific
495 position in the images and the length of the arrow indicates the corresponding anisotropy
496 magnitude. Length of one arrow is labeled in the each of the quiver plots to show the scale. All
497 quiver plots are generated in the same scale for easier comparison.

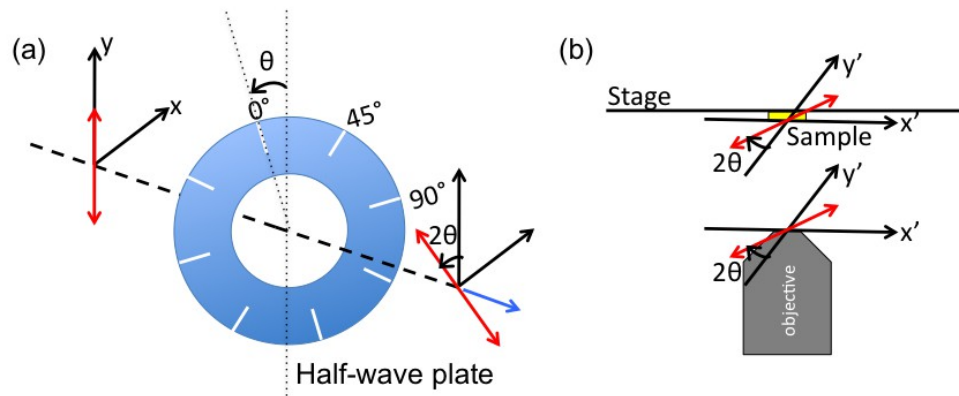
498

499

500

501

502 **Figure 1**



503

504

505

506

507

508

509

510

511

512

513

514

515

516

517

518

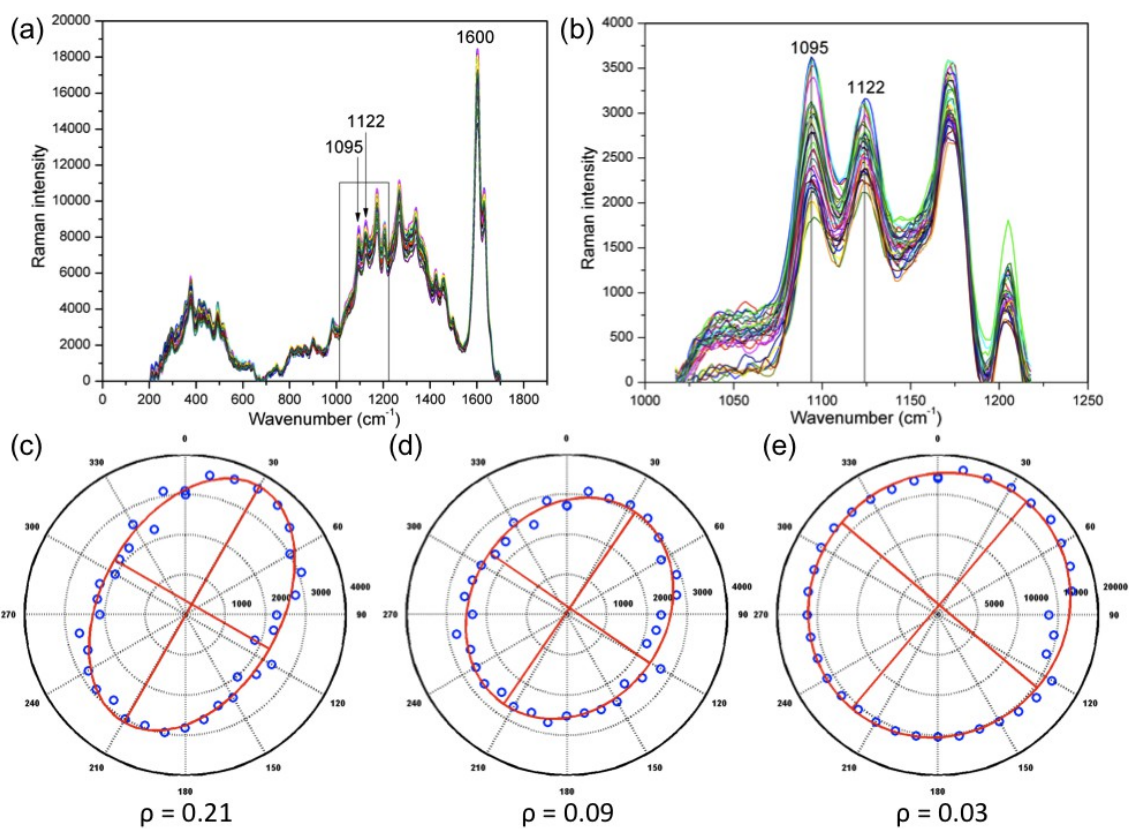
519

520

521

522

523 Figure 2.



524

525

526

527

528

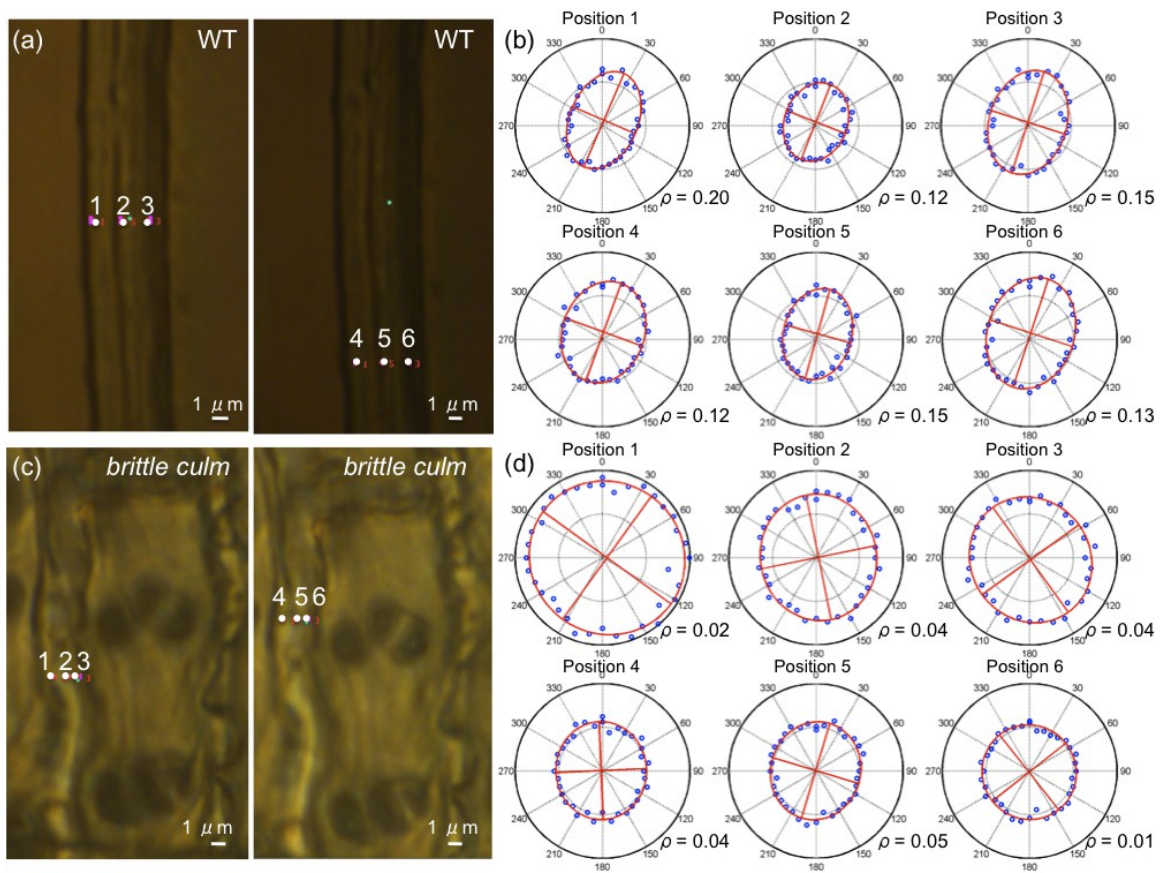
529

530

531

532
533
534
535
536
537

538 **Figure 3**



539
540
541
542
543
544

545

546

547

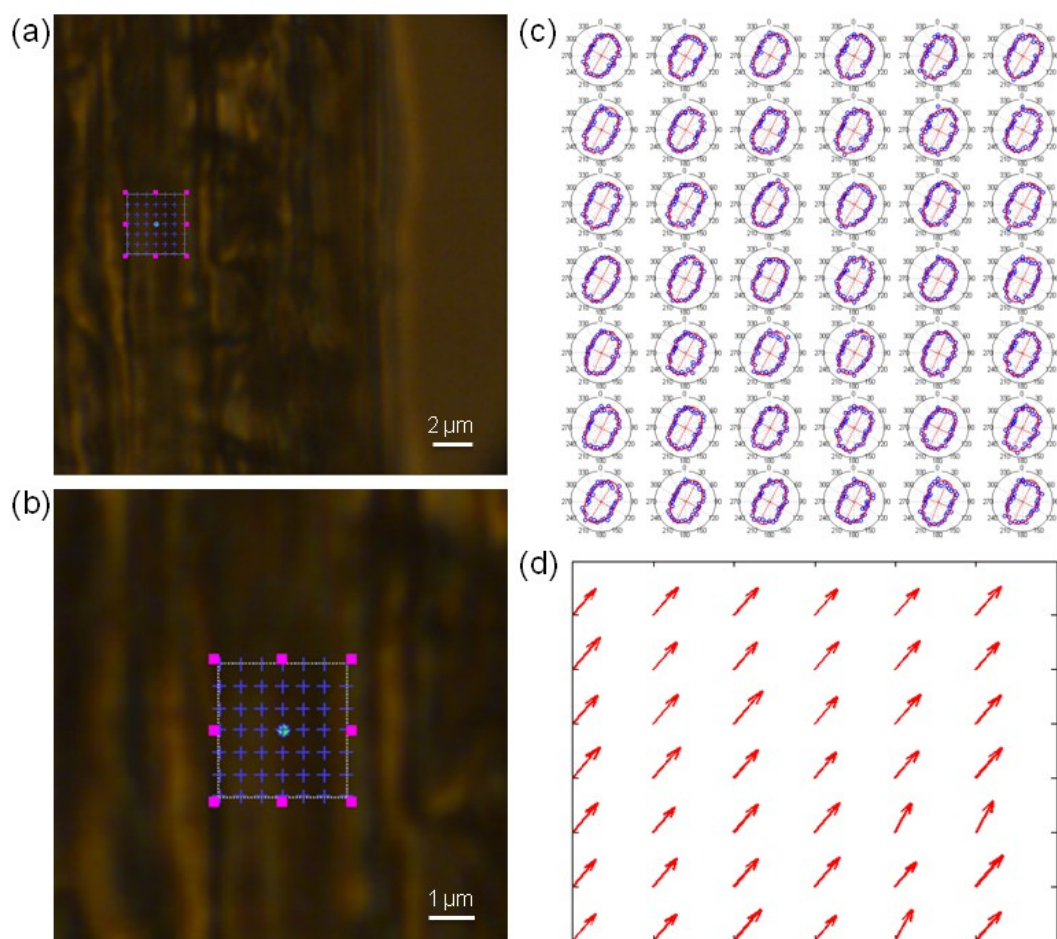
548

549

550

551

552 **Figure 4**



553

554

555

556

557

558

559

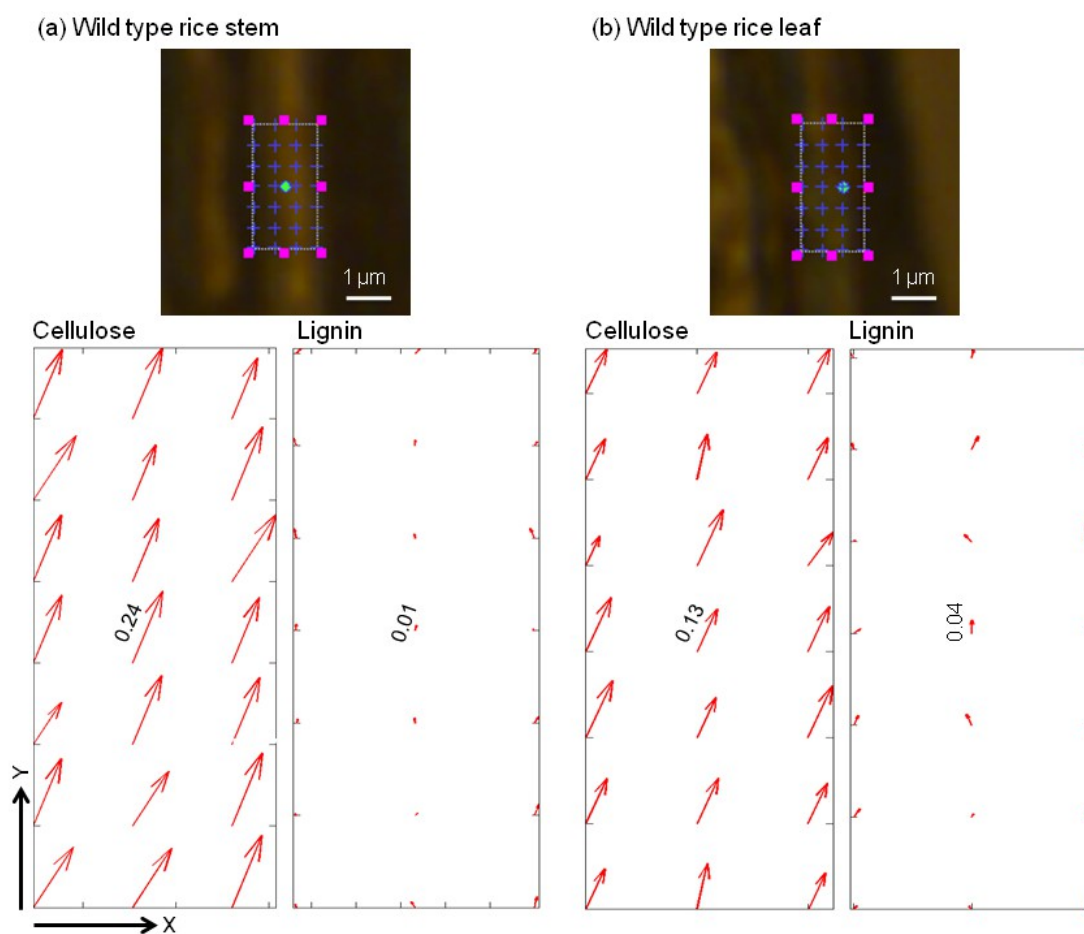
560

561

562

563

564 **Figure 5**



565

566

567

568

569

570

571

572

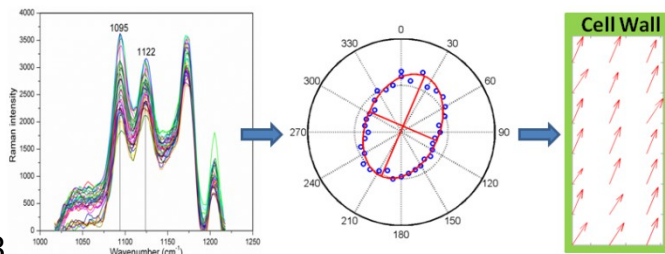
573

574

575

576

577 Table of Contents Graphic



578

579 The authors developed a noninvasive polarized Raman microspectroscopic method to determine

580 distribution of cellulose microfibril orientation within rice plant cell walls. Clear differences in

581 cellulose microfibril orientation were observed between different tissues of the wild type rice

582 plant as well as between the wild type and the *brittle culm* mutant, a mutant compromised in

583 secondary cell wall deposition. This is the first time that polarized Raman microspectroscopy

584 was used to determine supramolecular organization in cell walls for herbaceous plants.

585